
# In-situ X-ray analysis of cold alkali dissolution of cellulose pulps of various origin

Cellulose (2025) 32:115–131
https://doi.org/10.1007/s10570-024-06235-7

ORIGINAL RESEARCH

# In-situ X-ray analysis of cold alkali dissolution of cellulose pulps of various origin

**Joanna Wojtasz · Jenny Bengtsson · Hanna Ulmefors · Diana Bernin · Åsa Östlund · Shun Yu**

Received: 17 April 2024 / Accepted: 18 October 2024 / Published online: 25 November 2024


**Abstract** This article elucidates the dissolution of cellulose from different raw materials in NaOH aqueous solution via the combination of synchrotron-radiation-based SAXS/WAXS characterization. The X-ray measurements probed the mesostructure of the cellulose samples during the freeze-thawing cycle allowing tracking the initial swelling of the structure, the kinetics of disintegration of the cellulose crystallites as well as controlling the final state of the cellulose solution, i.e. presence or absence of cellulose aggregates. The individual SAXS and WAXS measurements were fitted and modelled to enable visualisation and tracking of the changes in the structure in relation to temperature during cooling and warming phases. To further increase the understanding of the parameters affecting dissolution different cellulose samples and solution compositions were considered. For this purpose the effect of increasing the concentration of NaOH and adding $Zn^{2+}$ has been carefully investigated as well as the importance of the cellulose origin. We found consistent development that the dissolution occurs faster at higher concentrations of NaOH and with $Zn^{2+}$ regardless the origin. Nevertheless, SAXS data show that materials with a larger amount of cellulose I show more apparent swelling in mesoscopic structure than bleached agricultural containing cellulose II. Despite

**Supplementary Information** The online version contains supplementary material available at https://doi.org/10.1007/s10570-024-06235-7.

J. Wojtasz
Department of Chemistry and Chemical Engineering, Chalmers University of Technology, 412 96 Gothenburg, Sweden

*Present Address:*
J. Wojtasz
TreeToTextile AB, Entreprenörsstråket 10, 431 53 Mölndal, Sweden

J. Bengtsson · H. Ulmefors
Fiber development, Department of Polymer, Fiber and Composites, RISE Research Institutes of Sweden, Argongatan 30, 431 53 Mölndal, Sweden

*Present Address:*
H. Ulmefors
Chalmers Industriteknik, 412 58 Gothenburg, Sweden

D. Bernin
Department of Chemistry and Chemical Engineering, Chalmers University of Technology, 412 96 Gothenburg, Sweden

Å. Östlund
TreeToTextile AB, Box 190, 101 23 Stockholm, Sweden

S. Yu
Material, Surface and Barriers, Department of Sustainable Materials and Packaging, RISE Research Institutes of Sweden, Scheelevägen 17, 22363 Lund, Sweden

S. Yu (✉)
LINXS Institute of Advanced Neutron and X-ray Science (LINXS), Lund, Sweden
e-mail: shun.yu@ri.se

few crystalline residues after the complete cooling-heating cycle shown by WAXS, some cellulose was not completely dissolved as some network structure remained in the samples under the test condition as suggested by SAXS.

**Keywords** SAXS/WAXS · Crystalline · Fiber network

## Introduction

The global demand of textile fibers, and man-made cellulose fibers (MMCF) in particular, is expected to increase substantially in the coming decade. At present time, MMCF are primarily produced from wood based cellulose using the viscose process (The Fiber Year 2022). Although both the viscose and lyocell process, the largest MMCF production methods, can result in lower environmental impact than production of synthetic fibres (Shen et al. 2010), the processes are also associated with different challenges. The viscose production is burdened with high ecotoxicity and the lyocell process has severe safety concerns and high energy consumption from dissolution and solvent recovery (Guo et al. 2021). Thus, motivated by environmental and economical factors, there is a continuous search and many ongoing activities on alternative manufacturing processes (Mendes et al. 2021; Kim et al. 2022).

Dissolution of cellulose in aqueous NaOH has a great potential in rendering an inexpensive cellulose fiber with low environmental impact. The solvent system is however coupled with some challenges and to ensure industrial feasibility, a deep understanding of the different process steps is essential (Tu et al. 2022).

Dissolving pulps from hardwood or softwood are the most common raw material for MMCF, followed by cotton linters. However, cotton production is limited and wood may not be sufficient to cover the biomass demand in the future resulting in a so called "cellulose gap" (Haemmerle 2011). Therefore, other sources needs to be considered. Increasing commercial and research activities are directed to evaluating many different alternative cellulosic raw materials for MMCF. An interesting option is untapped resources, such as paper-based and textile waste (Ma et al. 2018; Määttänen et al. 2021) as well as agricultural residues such as straw or oat husks (Essity 2021; Jahan et al. 2018; Wojtasz et al. 2024). This is pursued also in this work, where non-wood pulps are included.

This study aims to analyze the initial process step in MMCF manufacturing: the dissolution of cellulose. Successful dissolution of cellulose requires that the hydrogen bonds and the hydrophobic interactions in the solid-state are disrupted by the solvent and new hydrogen bonds are formed in case of an aqueous solvent (Lindman et al. 2017). The entropic gain upon dissolution is not a major factor for a rigid polymer such as cellulose (Budtova and Navard 2016). In aqueous NaOH the hydrophobic interactions are believed to be partly interrupted due to ionization of the cellulose in strong alkali (Bialik et al. 2016). Characterization of cellulose-NaOH(aq) dissolution using small angle X-ray scattering (SAXS) has been reported in the literature, but is often based on pre-mixed samples of microcrystalline cellulose (MCC) as a model for cellulose (Martin-Bertelsen et al. 2020; Swensson et al. 2021). In line with other solvents cellulose dissolution in cold alkali will be highly dependent on the degree of polymerization of the cellulose (Vallejos et al. 2022; Koistinen et al. 2023). Activation and pretreatment of the cellulose pulp can be used to aid dissolution in aqueous NaOH. For example, enzymatic treatment of pulp with cellulases was found to increase solubility in NaOH/ZnO (Vehviläinen et al. 2015). Here, the behaviours of different cellulose samples, e.g. MCC, pre-hydrolyzed celluloses and commercial pulps were studied to provide a broader understanding.

The solvent should also prevent self-aggregation, i.e. formation of persistent interactions or crystallisation, of cellulose chains over time. Various additives have been added to aqeuous NaOH to improve both the cellulose dissolution and the stability of the cellulose solution (Viäsnen et al. 2021; Davidson 1937). For instance, addition of ZnO and urea has been found to delay the gelation of a cellulose-NaOH-ZnO solution (Liu et al. 2011; Cai and Zhang 2005).

Analysis of the dissolution of cellulose in aqueous NaOH has been previously conducted using different methods. Mapping of the cellulose dissolution at low temperatures has been performed with NMR (Gunnarsson et al. 2019; Alves et al. 2016). The aggregation of different concentrations of cellulose in aqueous NaOH solution has been studied with small angle X-ray scattering (Martin-Bertelsen et al. 2020). In the

current study the rapid dissolution of cellulose in aqueous NaOH, with and without addition of ZnO, was efficiently studied with simultaneous SAXS/WAXS enabled by the high photon flux at the synchrotron radiation facility. The methodology used within the study enabled the dissolution process, in terms of crystalline disintegration and fibrillar aggregation state, to be followed from ambient temperature down to freezing of the solution. Several sources of cellulose were included to study its impact on dissolution.

## Materials and methods

### Materials

MCC Avicel PH-101 was purchased from FMC BioPolymer and used without further treatment.

Birch (Betula pendula) prehydrolysis Kraft pulp (476 $cm^3/g$, DP = 1133, Mn = 65.9 kDa, Mw = 269.3 kDa, polydispersity index 4.1) and Enocell Speciality Cellulose, Finland was used fluffed. Enocell has been acid hydrolysed to 200 $cm^3/g$. The two pulps are further referred to as IV 400 and IV 200.

Bleached oat and wheat pulps were produced on a laboratory scale by acid extraction followed by soda pulping and OQPP bleaching sequence. Pretreatment, cooking and oxygen bleaching were performed in 1.5 L steel autoclaves rotating at 15 rpm within a thermostated PEG bath and followed by EDTA chalating and peroxide bleaching performed in polyethylene bags placed in water baths as described by Wojtasz et al. (2024). After each step the pulp was carefully washed and a sample was taken for analysis. The obtained pulps contained 96.6 and 96.3% cellulose, 2.1 and 2.3% hemicelluloses and 0.3 and 0.5% Klason lignin. It was shown that a fraction of cellulose II was present in both the materials as a result of oxygen bleaching step. The pulps were hydrolyzed down to IV 200 with 1 M HCl.

1 M HCl, 50% NaOH solution of analytical grade (Merck) and ZnO (UnivarSolutions) were used without further purification.

### Methods

#### *Solvent composition*

The concentrations of NaOH and ZnO were chosen based on previously published study (Vehviläinen et al. 2015). In summary, three different solvent compositions were selected: 6.5 wt% NaOH, 6.5 wt% NaOH with 1.3 wt% ZnO, and 4.0 wt% or 3.25 wt% NaOH with 0.65 wt% ZnO.

#### *Sample preparation*

The non-wooden cellulose from different sources was ground/made into powder to enable smooth sample handling for the synchrotron measurements.

The cellulose was added to a thin-walled quartz capillary (diameter 1.5 mm, wall thickness 0.01 mm), and the capillary was subsequently filled with solvent. Weighing of the capillary before and after each step ensured a cellulose concentration in the range of 2.6—3.0 wt% for all samples.

#### *X-ray scattering*

In situ SAXS/WAXS were performed at P62 SAXSMAT beamline at PETRA III storage ring, DESY, Hamburg. The X-ray energy is 12.4 keV with SAXS sample-to-detector distance of around 2.5 m and WAXS detector at about 117 mm, covering a q range of 0.1—4.5 $nm^{-1}$ for SAXS and 10.0—36.0 $nm^{-1}$ for WAXS (seen in Fig. 1. An Linkam heating/cooling stage was used to control the temperature. At the given geometry, no apparent anisotropicity has been observed in either the SAXS or WAXS 2D patterns. Only 1D profiles extracted from the 2D pattern by PyFAI algorithms have been analyzed (Ashiotis et al. 2015).

#### *Data analysis*

The experimental concept and data analysis are summarized in Fig. 1. By following the temperature profile Fig. 1 a , SAXS and WAXS patterns were collected as shown in Figs. 1 b and c . In some runs ice formed around -20 °C or below (not shown in the Figures). The backgrounds of SAXS were measured for all NaOH solutions with/without ZnO during the cooling and heating cycles. The structural information contained in the SAXS was extracted via curve fitting and necessary background correction. For the dissolution experiments, the SAXS profile is subtracted from the corresponding background of the same solutions and at the nearest temperature of the corresponding cooling/heating cycles. This is valid

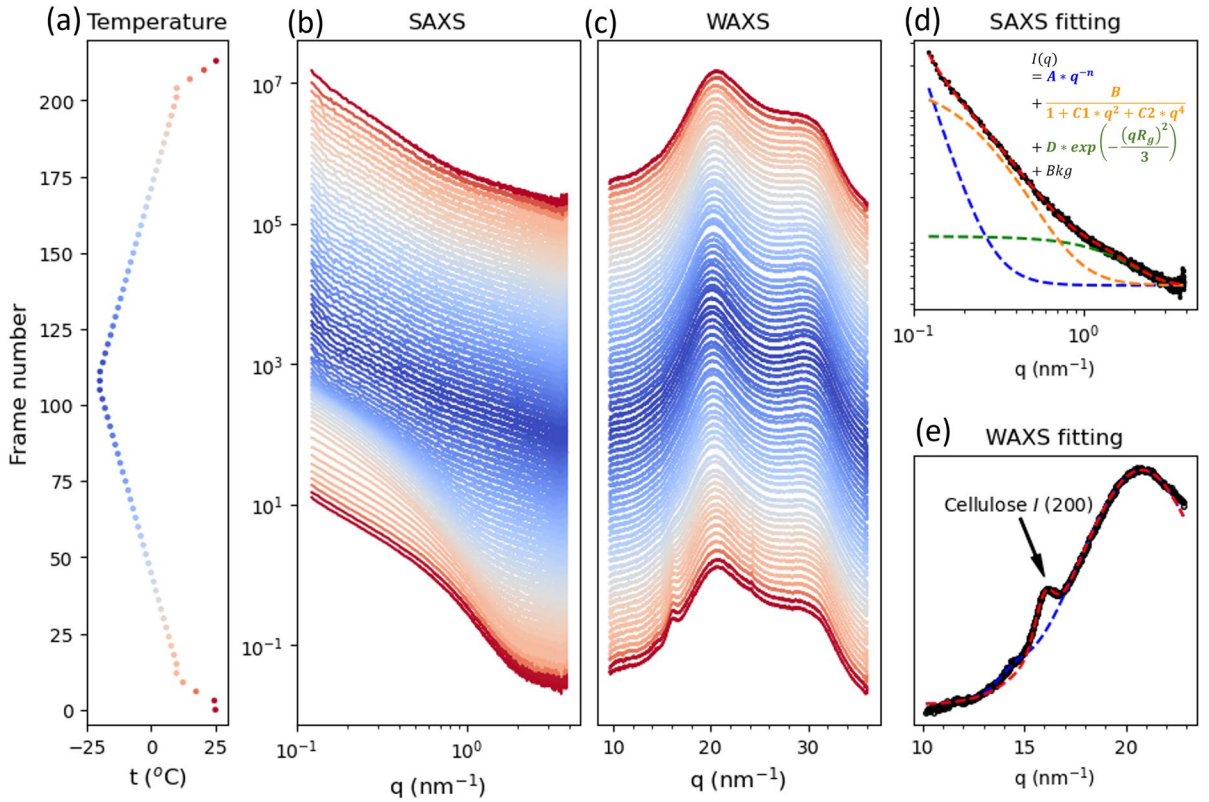


**Fig. 1** **a** Temperature profile with the corresponding SAXS **b** and WAXS **c** profiles of MCC in 6.5% NaOH. The examples of curve fitting of SAXS **d** and WAXS **e** of MCC (cellulose I crystalline structure)

because the background of solutions often only shifts the baseline intensity in the SAXS region. However, the background removal of WAXS might not always be straightforward due to the less defined contribution of the amorphous phase from the material/solvent systems and the surroundings and shadows of the sample environments. Instead, WAXS analyses are focused on the apparent Bragg peaks with all other disorder contribution fitted via a broad Voigt peak with a flat background as the baseline. In this case, the trends of developing Bragg peak fitting parameters are still reliable. Figure 1 d and e show curve fitting results of selected SAXS and WAXS line profiles, respectively.

The small angle X-ray scattering provides information on the hierarchical structure of the material changes on the nanoscale during the dissolution. The SAXS profile analysis and modeling of cellulose materials is a rich field with many approaches applying to diluted nanocellulose suspension (Mao et al. 2017), nanocellulose gel (Guccini et al. 2018), highly oriented fiber (Gubitosi et al. 2021) and wood (Penttilä et al. 2019), and hierarchical pulp systems (Cheng et al. 2015). In general, well-defined geometric structures, e.g. ribben (Mao et al. 2017) or cylinders (Gubitosi et al. 2021; Penttilä et al. 2019), apply for the diluted and oriented system, while empirical models based on analytical functions is often used for multiscale system (Guccini et al. 2018; Cheng et al. 2015). In this case, our pulp materials are condensed systems showing isotropic hierarchical structure in the scattering pattern. So, we conform to an empirical model consisting of multiple functions accounting for multiscale structures in equation 1.

$$I_{SAXS}(q) = A * q^{(-n)} + \frac{B}{\left(1 + C_1 * q^2 + C_2 * q^4\right)} + D * exp\left(-\frac{\left(qR_g\right)^2}{3}\right) + Bkg \quad (1)$$

$$\xi = \left[\frac{1}{2}C_2^{-\frac{1}{2}} + \frac{C_1}{4C_2}\right]^{-\frac{1}{2}} \quad (2)$$

Different terms of the right side of equation 1 correspond to the contributions of structures at different scales, whose dominant contributions were clearly illustrated in Figure 1 (d): the first term, the power law contribution, originates from the fractural nature of the particle system (Porod 1949) with common interpretation as a smooth surface of an object with a sharp interface if the exponent is 4, also known as Porod's law (Ciccariello et al. 1988); the surface fractals of large objects if the exponent is between 3 and 4 (Mildner 1986; Schmidt 1991); or aggregates with mass fractals geometry if the value is between 1 and 3 (Teixeira 1988). The second term is Teubner-Strey model (Teubner and Strey 1987). It was developed to model the bicontinuous microemulsions (Schmidt et al. 2023) and weakly structured gels (Xi et al. 2021), and has been generalized for mesoporous structure (Saurel et al. 2019). It should be noted that Teubner-Strey model is a model originally derived from a space correlation function consisting exponential decay and trigonometric sine function and the correlation length $\xi$ could be calculated via Equation 2. In our case of cellulose soaked in the solution, it serves as a good approximation to include the fiber correlation in the nanoscale, a similar approach of which has been used by Penttilä et al (Penttilä et al. 2013). The third term, Guinier model, accounts for any small object with a radius of gyration of $R_g$ appearing upon dissolution (Guinier 1955).

WAXS detects the Bragg peaks due to scattering by the crystalline structure of the material. Cellulose I (200) peak of MCC and pulps (as shown in Fig. 1 e and that mixed with cellulose II (020) contribution from bleached oats and wheats (not present in Fig. 1) could be captured despite an enormous background from the solution. Nevertheless, it is very challenging to use the atomistic-model-derived peaks fitting to deconvolute the contribution of cellulose II from that of cellulose I. Thus, the WAXS curves were fitted by using a sum of multiple Voigt functions (Eq. 3 ) to reproduce the intensities of the crystalline peaks for each measurement during the freezing/thawing sequence. During complete dissolution, it is expected that the crystalline peaks disappear due to the disruption of the crystalline order of cellulose chains. From the WAXS data, this disintegration of the crystalline domains could be extracted with respect to temperature.

$$I_{WAXS}(q) = \sum_{n=1}^{3} c_n * Voigt\left(q_{peak}^n, W_G^n, W_L^n\right) + Bkg \quad (3)$$

where $c_n$ is intensity coefficient, $q_{peak}^n$, $W_G^n$ and $W_L^n$ are the $n^{th}$ Voigt function's peak position, Gaussian and Lorentzian width, respectively.

*Solid-state nuclear magnetic resonance (NMR)*

$^{13}$C solid-state cross-polarization (CP) NMR experiments were recorded on a Bruker Avance III 500 MHz spectrometer equipped with a 4 mm HX CP MAS probe. The Zirconia rotors were spun at 10 kHz and the temperature was set to 298 K. $^{1}$H decoupling with a 'spinal64' decoupling scheme at 67 kHz was applied during the acquisition. The CP duration was set to 1.5 ms and the repetition time to 2 s.

*Microscopy*

The dissolution was also followed with optical microscopy by use of ZEISS SteREO Discovery.V12 microscope equipped with a LINKAM themperature control stage.

## Results

The structure of raw materials

A quality check of the cellulose raw materials from different origins has been conducted by using WAXS (Fig. 2) and solid state NMR (Fig. 3). WAXS Braggs peaks of raw materials are shifted to highlight the variation of the crystalline phases with the theoretical model of cellulose I (Fig. 2 top) and cellulose II (Fig. 2 bottom) as the references. The appearing profiles of MCC, Pulp IV 200, and Pulp IV 400 resemble cellulose I structure, while bleached Oat and Wheat show features of cellulose II. In general, natural pulps do not possess cellulose II structure. The cellulose II components may be developed during the pulping/bleaching cycles. To quantify the contribution of cellulose I and cellulose II requires sophisticated peak deconvolution, which is beyond the scope of this

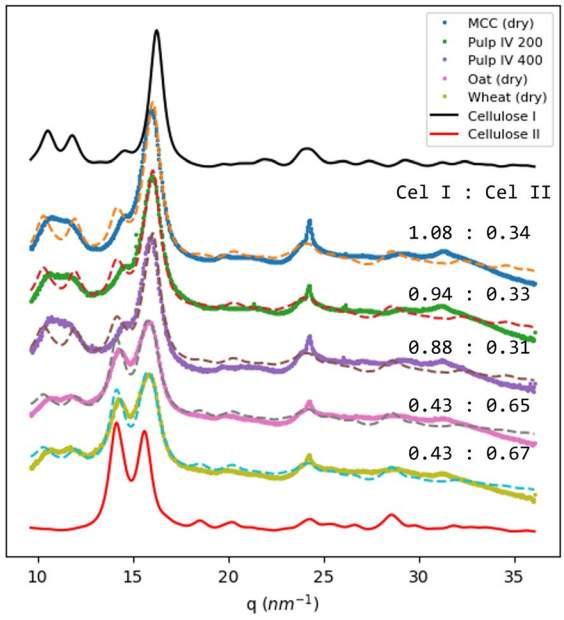


**Fig. 2** WAXS on dry materials, the dashed line are the best fit made of a linear combination of the model cellulose I and cellulose II structure, The fitting factor of cellulose I (Cel I) and cellulose (Cel II) are shown next to the fitting results

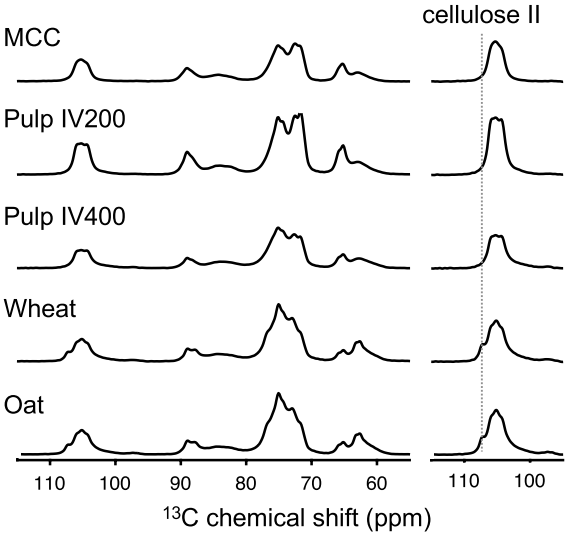


**Fig. 3** $^{13}$C solid-state CP NMR spectra for MCC, pulps IV200 and IV400, bleached wheat and oat to the left. To the right, the spectra show the C1 peak. The peak shape and position indicates the presence of cellulose II (see dashed line)

work. Nevertheless, a quick linear combination fitting of the references cellulose I and cellulose II could qualitatively show the occurrence of the increased cellulose II components as the relative fitting factor of cellulose II increases compared to cellulose I. In the later section of in-situ dissolution characterization, WAXS analyses focus on the cellulose I (200) reflections of MCC and pulps, and the peak overlapped with the theoretical positions of cellulose I (200) and cellulose II (020) for bleached oat and wheat. To further confirm the presence of cellulose II in bleached oats and wheats, solid-state NMR was performed. In the right penal of Fig. 3, a dashed line around 107 ppm guided the comparison of solid-state NMR C-1 signals from different raw materials, and the shoulder peaks of the bleached oat and wheat is a characteristic feature of cellulose II (Zuckerstätter et al. 2009).

## Dissolution of MCC

As a reference, a well studied cellulose system was investigated, namely MCC in alkali. MCC is often used as a model for cellulose behaviour, even though its behavior cannot be directly translated to that of cellulose pulps, due to its lack of fibrous structure and high relative crystallinity. Nevertheless, this reference system helps to gain a general understanding of the process and allows us to relate the current study to the ones reported in the literature earlier using MCC (Martin-Bertelsen et al. 2020; Swensson et al. 2021; Gunnarsson et al. 2019). To gain further understanding of the dissolution mechanisms, measurements were made with different solvent compositions: 6.5% NaOH, 6.5% NaOH with 1.3% ZnO to ensure improved dissolution, although the role of the ZnO in solution is debated (Kihlman et al. 2013; Liu et al. 2011; Viäsnen et al. 2021), and the diluted solvent with 3.25% NaOH and 0.65% ZnO.

From the collected WAXS data, the intensities of the crystalline peaks during the freezing/thawing sequence were obtained and plotted with respect to temperature, as shown in Fig. 4 (d). For the concentrated solvents with 6.5% alkali with/without ZnO (blue/black curves), the intensity of those peaks decreases when the solution is cooled down in both cases, indicating a gradual disintegration of the crystalline structure. Interestingly, the decay starts already at around 10°C and the significant drop in crystalline signal is observed at

5°C, showing a faster decay rate with ZnO addition. Between 5°C, and -5°C the peak almost disappeared, indicating disintegration of the crystalline phase, and only a 10% intensity remained at temperatures below −10°C. Thawing the sample and reheating to 20°C did not result in any change in the peak intensity, indicating that the dissolution process was non-reversible and reached an equilibrium state in the cooling down phase for the 6.5% NaOH solutions. Noteworthy is also that in our experiment the concentrated MCC/NaOH solution did not freeze when cooled to -20 °C. This was expected as earlier research showed that the freezing pattern of the alkali solution is affected by presence of MCC (Gunnarsson et al. 2019). After thawing the signal from the crystalline peak for the solutions containing 6.5% NaOH is close to zero, however it did not disappear totally with some residual crystalline peak signal persisting. This residual signal could be partially related to a fitting artifact. The role of the ZnO has been investigated via Raman spectroscopy by Väisänen et al., and suggested as "that the addition of ZnO to aqueous NaOH aids the dissolution of cellulose and hinders its self-aggregation in solution by coordinatively binding to the C2 and C3 OH groups of the cellulose chains deliberated from the crystalline structure and thus forming a ring-like structure similar to zinc glycerolate" and "even with the addition of ZnO, a temperature below 0 °C is required to dissolve cellulose"(Viäsnen et al. 2021). Despite the lack of chemical insights, WAXS provides complementary information on the crystalline phase during the dissolution. In Fig. 4 h , the peak width development shows that without the addition of ZnO the peak width became broader upon cooling; on the contrary, the increase of ZnO percentage will lead to narrower width. Such observation is also seen for Pulp IV 200 (Fig. 8) and bleached agricultural cellulose (See supplementary information) in the later sections. Under the frame of the Debye-Scherrer equation, such a peak width change could be interpreted as that the NaOH treatment disintegrates crystalline into smaller domains before dissolving them, while the addition of ZnO induces the formation of larger crystalline domains before their dissolution. Such observation might also be interpreted as that the binding of Zn to the edge of cellulose fibrils links adjacent fibrils, aligning the crystalline domains for a sharper peak.

In the diluted solutions, 4% and 3.25% NaOH with 0.65% ZnO, showed a different behaviour—it shows a slower peak decay rate is observed as a function of the concentration during cooling down and before their sharp peak intensity drops around −18°C (red/green curve in Fig. 4 d) owing to the ice formation. The slower decay may be understood as that cellulose is well charged in lower concentrations of NaOH, which is suggested as key factor by Lindman et al. (Lindman et al. 2017). Based on the observation, the concentration of NaOH is a dominant factor to initiate the dissolution over the addition of ZnO. Furthermore, when the ice melted the crystalline peak intensities of samples in 4% and 3.25% NaOH as well as with 0.65% ZnO had also been reduced to levels comparable to those of the 6.5% NaOH solutions. It thus remains unknown how dissolution took place in the presence of ice.

Figure 4 a-c present the intensity parameters extracted from the fitted SAXS results for power-law, Teubner-Strey model and Guinier-like contributions, respectively. For systems in 6.5% NaOH with/without ZnO (brown/black), as the dissolution progressed, the power-law intensity quickly decreased around 10°C, while the exponent also increased from around 2.7 to 4, suggesting that high-branched, also known as mass-fractal, larger structures/aggregates disappeared and smoothened out. It is also interesting to see a consistent rise in the normalized intensity of Teubener-Strey model at the beginning of the dissolution, which indicates an increase in occurrence of nanoscale network-like structure with the correlation distance shown in Fig. 4 f . As cooling continues, these network contribution decreased further, which could be explained through the disintegration of network structures. Such network development may be explained by swelling or ballooning which is commonly observed for celluloses in cold aqueous NaOH solutions (Lindman et al. 2017; Cuissinat and Navard 2006). A tentative scenario is that the specific zones where the swelling/ballooning takes place increases during dissolution, leading to an increase of the contribution to the scattering intensity. Then, when those zones are more connected at a later dissolution stage, the network structure is no longer similar to those in the initial stage, showing a decreased intensity. At smaller scales, objects with the radius of gyration of 1 nm started to appear. This is related to crystalline dissociation allowing cellulose chains to become mobile.

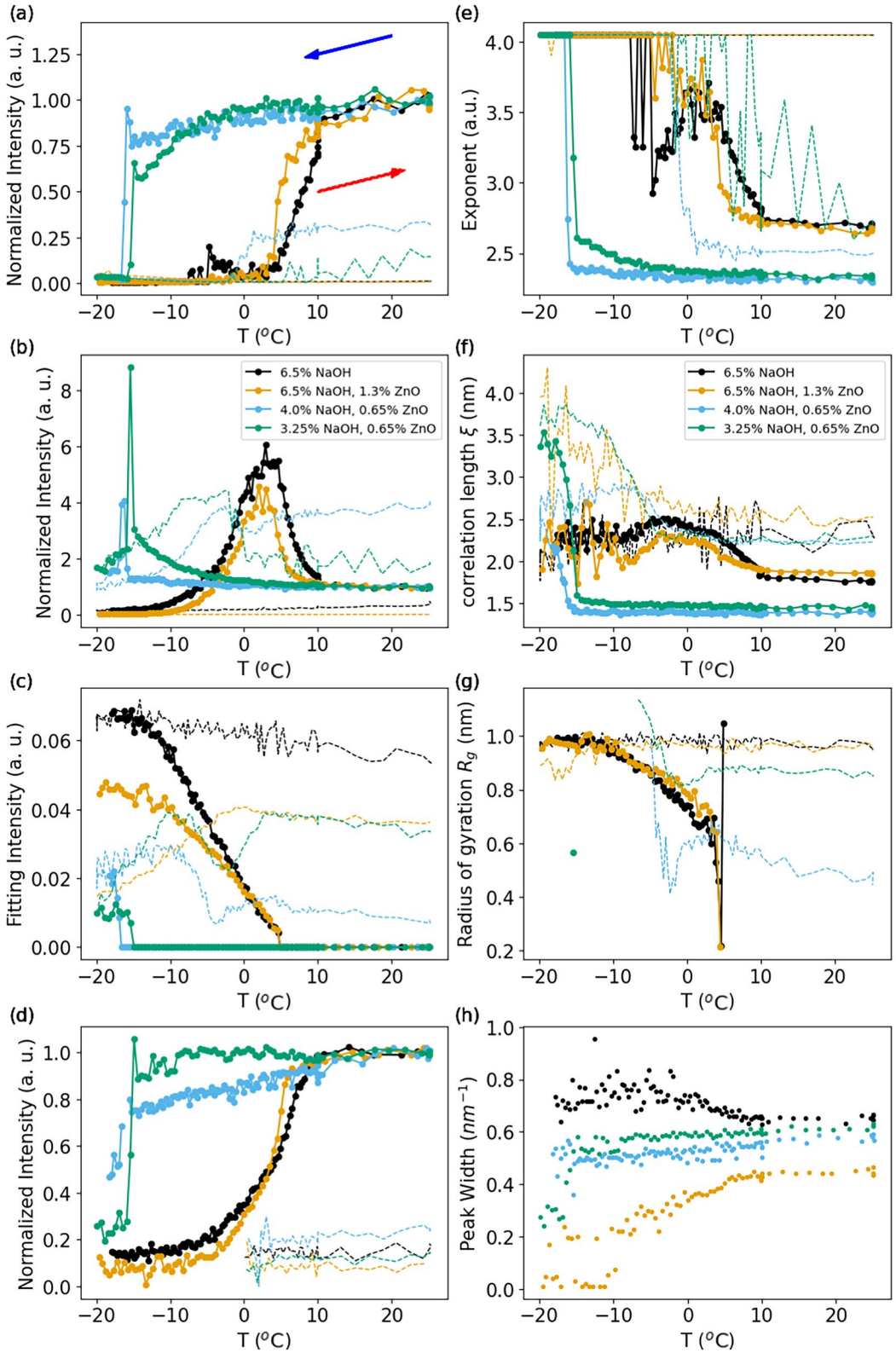
(a)
Normalized Intensity (a. u.)
T (°C)
(b)
Normalized Intensity (a. u.)
6.5% NaOH
6.5% NaOH, 1.3% ZnO
4.0% NaOH, 0.65% ZnO
3.25% NaOH, 0.65% ZnO
T (°C)
(c)
Fitting Intensity (a. u.)
T (°C)
(d)
Normalized Intensity (a. u.)
T (°C)
(e)
Exponent (a.u.)
T (°C)
(f)
correlation length ξ (nm)
6.5% NaOH
6.5% NaOH, 1.3% ZnO
4.0% NaOH, 0.65% ZnO
3.25% NaOH, 0.65% ZnO
T (°C)
(g)
Radius of gyration $R_g$ (nm)
T (°C)
(h)
Peak Width ($nm^{-1}$)
T (°C)

◂**Fig. 4** Summaries of SAXS and WAXS fitting parameters of MCC in 6.5% NaOH (black), 6.5% NaOH–1.3% ZnO (brown), 4.0%NaOH–0.65% ZnO (blue) and 3.25% NaOH–0.65% ZnO (green). **a**: the evolution of the intensity of the power law term in Equation (1) as a function of the temperature. The curve is normalized to the intensity at the beginning of the experiment. **b**: the evolution of the intensity of the Teubner-Strey model by similar normalization as **a**. **c**: the evolution of the intensity of the Guinier-depicted term without normalization. **d**: the evolution of the intensity of the WAXS (200) peak after normalization. **e**: the change of the exponent of the power law term. **f**: the correlation length of Teubner-Strey model calculated via Equation (2) with the fitting parameters. **g**: the fitted radius of gyration change as a function of temperature. (h): the evolution of the peak width of WAXS (200) peak. The solid lines with circles present the cooling cycles marked by the blue arrow in **a**, while the dashed lines stand for heating cycles marked by the red arrow in **a**

Despite Guinier modeling being dominant at higher q, a power-law exponent could be approximated to -1 for q larger than 1 $nm^{-1}$. This may suggest the existence of a stiff rod conformation of the chains that could be explained by the chains (partly) becoming mobile to go into the solution however not sufficient to reach the random coil confirmation. Similar observations were made by Martin-Bertelsen et al. (2020) and Swensson et al. (2021). All the SAXS evolution onsets are well correlated to the WAXS intensity's decay at around 10°C. For lower NaOH concentrations (4% red and 3.5% green), the network and Guinier-depicted encountered ice formation around -18°C. Overall, the SAXS/WAXS depicted the onset of swelling of the cellulose structure with hierarchical changes showing the crystalline disintegration, smaller object formation (Guinier), network opening/increase and smearing-out, as well as large structure dissolving.

Upon increasing temperature, the power-law and network contribution for MCC in 6.5% NaOH with/without ZnO are considerably smaller compared to before cooling but were still present after the freeze-thaw cycle. This residual large structure could be assigned to cellulose aggregates. A practical explanation for such a structure is the incomplete dissolution due to the lack of stirring. Without sufficient agitation, locally higher concentrations of cellulose in the suspensions could cause limited access to the solvent and lead to some agglomerated material remaining partially undissolved. In Fig. 4a and d, it indicates the beneficial effect of the presence of the ZnO favoring a faster dissolution rate and possibly fewer residual crystalline structures. The contribution of smaller objects depicted by Guinier-term reached a stable stage for both intensity and the radius of gyration (Fig. 4c and g), suggesting that the structure elements remain disintegrated. Some crystalline structures were also found for the diluted solvent but remained in the swollen/

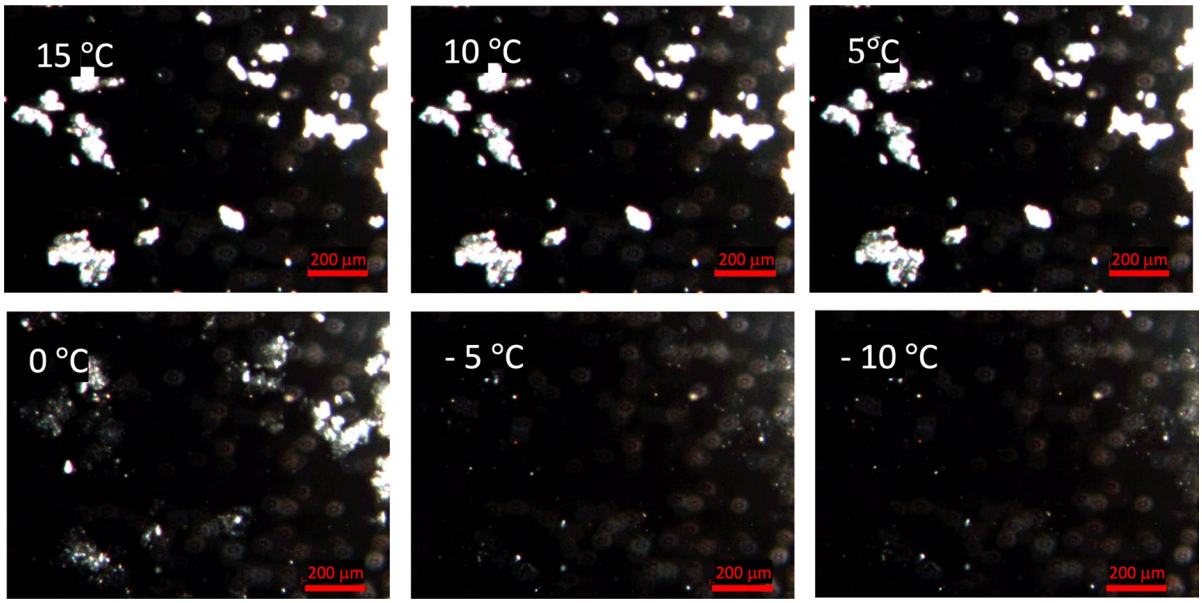


**Fig. 5** Microscopy images using a cross-polarizer of MCC dissolution in 6.5% NaOH(aq) with different temperatures

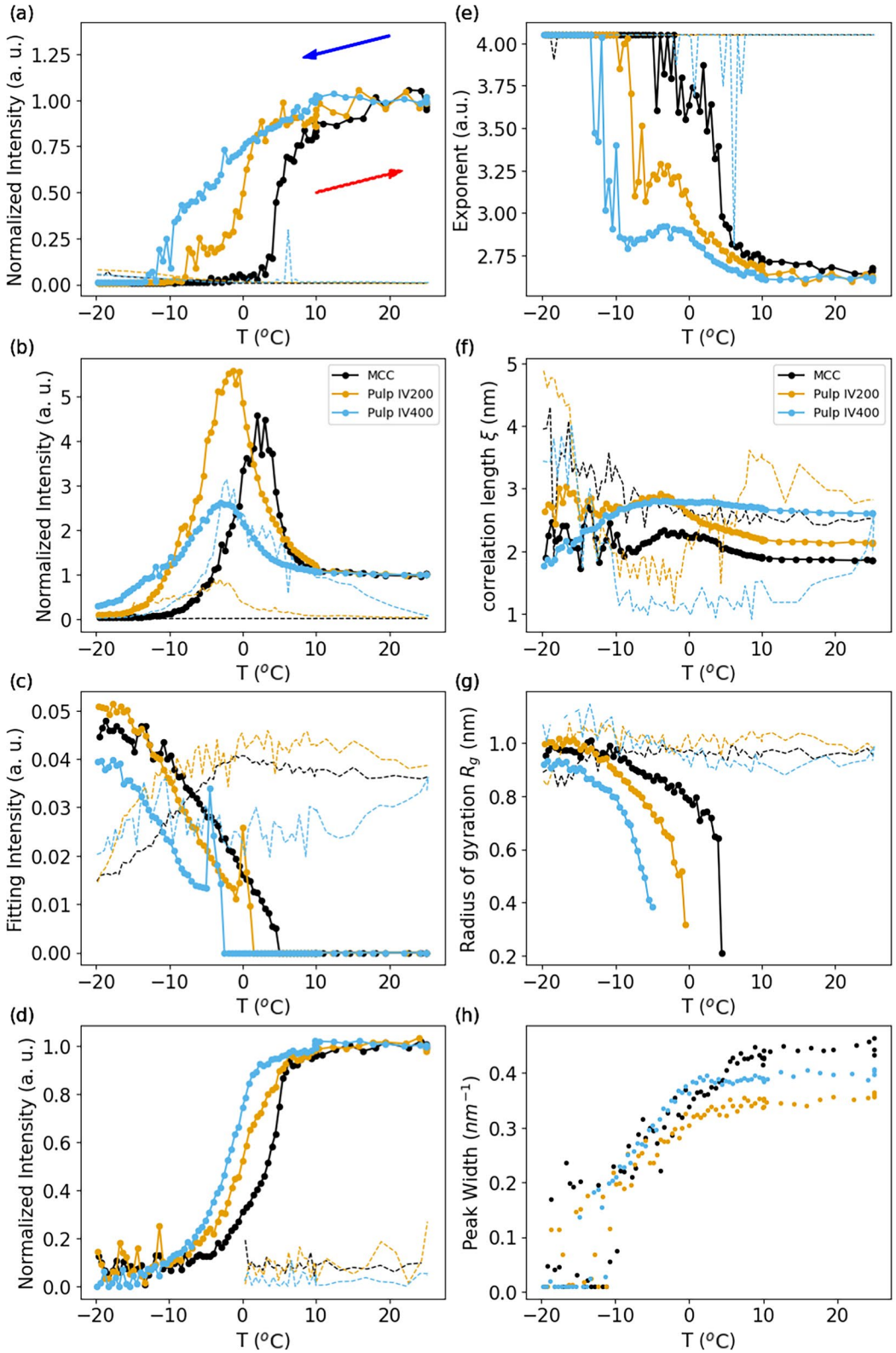
(a)
Normalized Intensity (a. u.)
T (°C)
(b)
Normalized Intensity (a. u.)
MCC
Pulp IV200
Pulp IV400
T (°C)
(c)
Fitting Intensity (a. u.)
T (°C)
(d)
Normalized Intensity (a. u.)
T (°C)
(e)
Exponent (a.u.)
T (°C)
(f)
correlation length ξ (nm)
MCC
Pulp IV200
Pulp IV400
T (°C)
(g)
Radius of gyration $R_g$ (nm)
T (°C)
(h)
Peak Width ($nm^{-1}$)
T (°C)

◂**Fig. 6** Summary of SAXS and WAXS fitting parameters of MCC (black), Pulp IV200 (brown) and Pulp IV400 (blue) in 6.5% NaOH–1.3% ZnO. **a-h** show the same parameters as those in Fig. 4 The solid lines with circles present the cooling cycles marked by the solid blue arrow in **a**, while the dashed lines stand for heating cycles marked by the red arrow in **a**

gel state as there is a significant contribution from the network structure (Fig. 4b blue and green dashed lines). It was assumed that for those samples a complete dissociation of cellulose chains did not occur. The reaggregation of the disintegrated crystalline structures could again be a plausible explanation, for example, the increase of temperature causes a decrease in cellulose solubility in this system but not sufficient to reform the crystalline phase. Nevertheless, it is interesting to see that in Fig. 4f, the residual networks (dashed lines) in all concentrations of NaOH show a similar correlation distance of around 2.5 nm in the solution, indicating a similar mesostructure.

The observation of non-dissolved cellulose in NaOH(aq) is in line with previous studies by Hagman et al. (2017), who used a combination of different methods (SAXS, NMR, light scattering and rheology) to study MCC in cold NaOH and showed that MCC can be fully molecularly dissolved in cold alkali however the final solution still shows concentration fluctuations consistent with significant attractive cellulose-cellulose interactions. Swensson et al. (2021), by using SAXS and NMR, also found a portion of undissolved cellulose in all of investigated NaOH(aq) cellulose solutions.

The dissolution of MCC in NaOH was also visualized with optical microscopy, and micrographs are presented in Fig. 5. The MCC was suspended in 6.5% NaOH solution and the temperature was decreased stepwise to −20°C and thereafter increased back to room temperature. By utilizing cross-polarizers, MCC with sustained structural integrity is easily observed. It can be seen that the dissolution behaviour captured with microscopy corresponds well to X-ray scattering results, especially the WAXS measurement. The onset of dissolution is visible below 5°C with a significant decrease in the amount of visible MCC between 5 and 0°C followed by a complete disappearance of the birefringent material at −5°C.

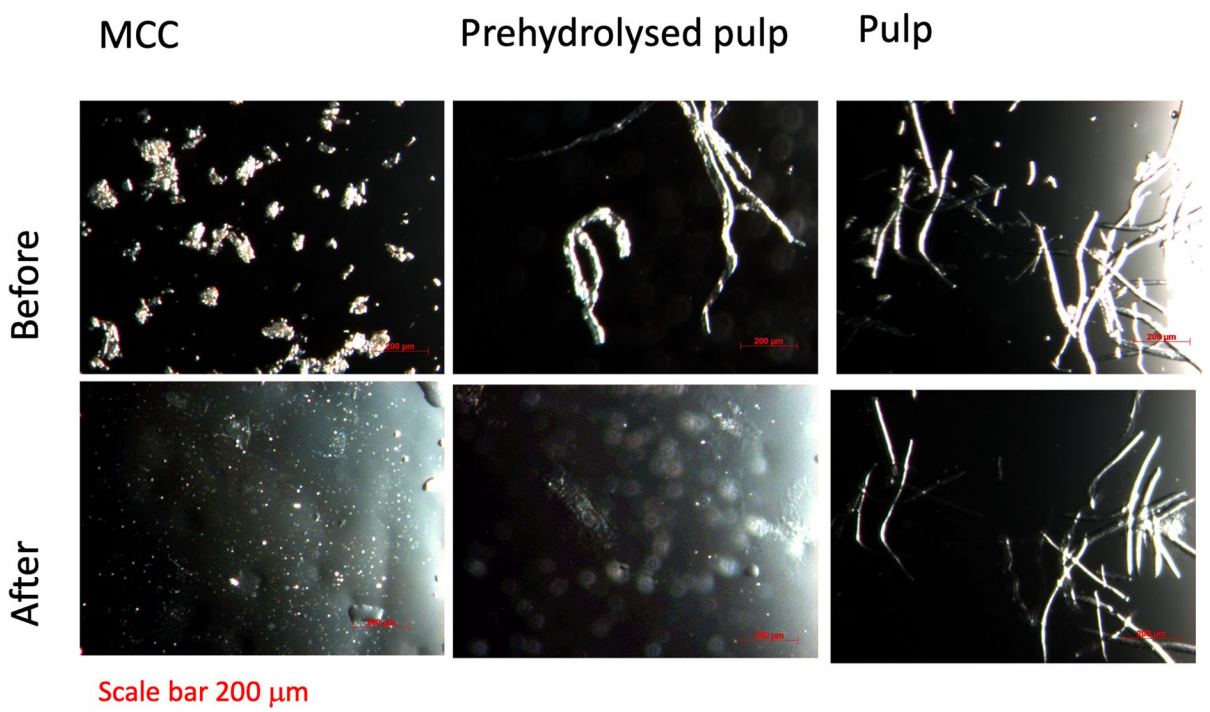


**Fig. 7** Microscopy pictures of pulps before and after freeze-thawing dissolutionFig.7 cycle in NaOH + ZnO

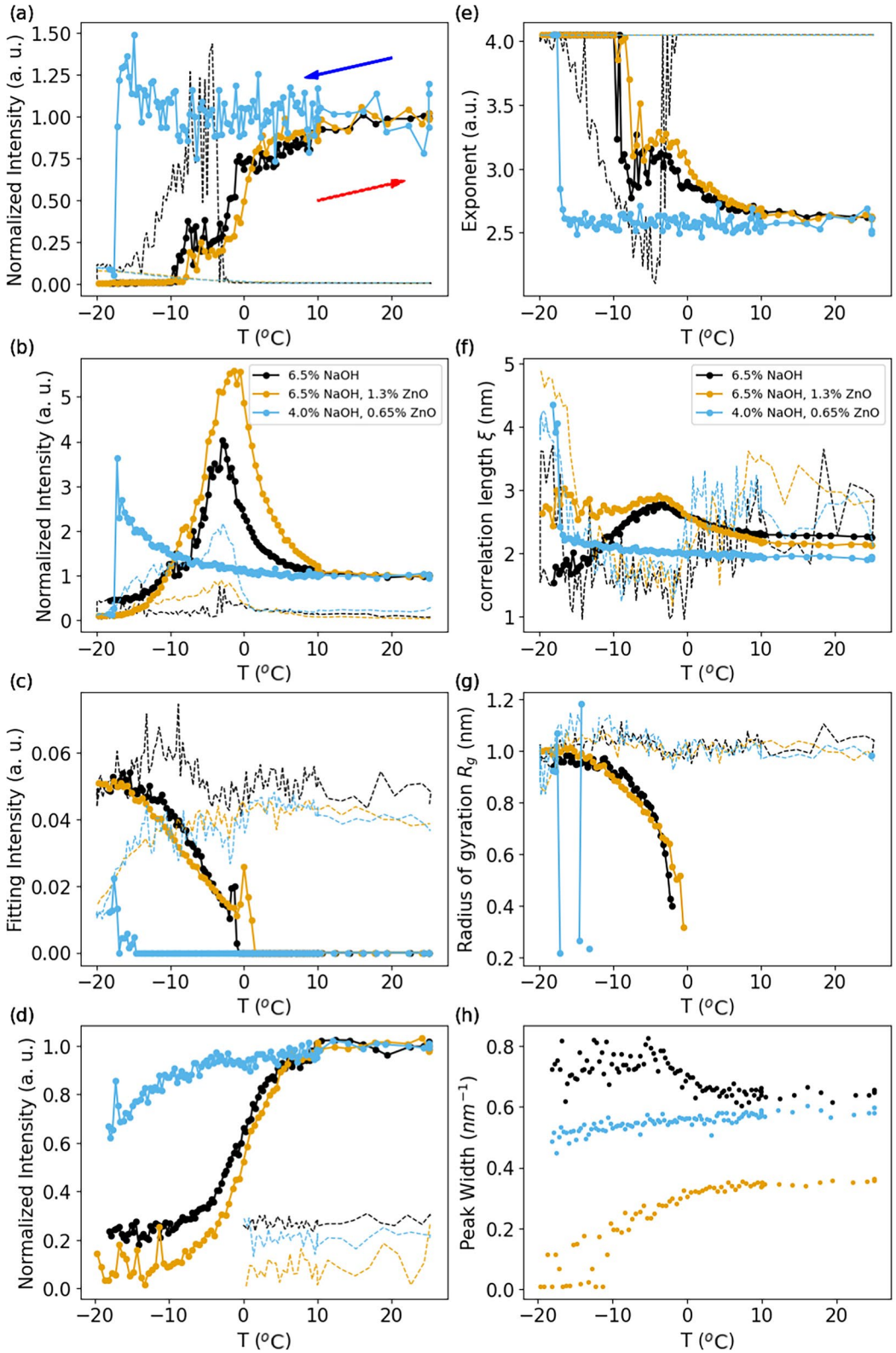
(a)
Normalized Intensity (a. u.)
T (°C)
(b)
Normalized Intensity (a. u.)
6.5% NaOH
6.5% NaOH, 1.3% ZnO
4.0% NaOH, 0.65% ZnO
T (°C)
(c)
Fitting Intensity (a. u.)
T (°C)
(d)
Normalized Intensity (a. u.)
T (°C)
(e)
Exponent (a.u.)
T (°C)
(f)
correlation length ξ (nm)
6.5% NaOH
6.5% NaOH, 1.3% ZnO
4.0% NaOH, 0.65% ZnO
T (°C)
(g)
Radius of gyration $R_g$ (nm)
T (°C)
(h)
Peak Width ($nm^{-1}$)
T (°C)

◂**Fig. 8** Summary of SAXS and WAXS fitting parameters of Pulp IV200 in 6.5% NaOH (black), 6.5% NaOH–1.3% ZnO (brown) and 4.0%NaOH–0.65% ZnO (blue). **a-h** shows the same parameters as those in Fig. 4 The solid lines with circles present the cooling cycles marked by the solid blue arrow in **a**, while the dashed lines stand for heating cycles marked by the red arrow in **a**

## Dissolution of cellulose fibres

MCC as a model for cellulose consists of relatively short cellulose chains. From an industrial perspective, a detailed dissolution of cellulose of higher molecular weight raises more attention i.e. in the production of MMCF. Therefore, the behaviour of a commercial pre-hydrolysis kraft pulp (PHK) dissolving pulp in cold alkali was studied in the same manner. For a better understanding of the importance of the cellulose chain length, the pulp was also hydrolyzed from a intrinsic viscosity of 400 to 200 $cm^3/g$.

Figure 6 presents the dissolution behaviours of two PHK pulps and a reference of MCC in 6.5% NaOH with 1.3% ZnO. SAXS (Fig. 6 a-c) and WAXS (Fig. 6 d) consistently indicate that the dissolution starts at a comparably higher temperature for MCC, followed by pulp with IV 200 and IV 400. It is consistent with the literature reports indicating that the dissolution temperature and the solubility of cellulose in alkali solvents is strongly related to the molecular weight and properties such as crystallinity (Qi et al. 2008).

The radius of gyration of the appearing smaller objects increased to 1 nm for all of pulps and MCC, suggesting the presence of similar structures in all samples independently on the pulp. However, more details about this structure requires complimentary characterizations and is beyond the scope of this work. For the mesoscale network, the maximum intensity suggests that more regions have swelled and then smeared out as seen in Fig. 6 b. Moreover, such swollen networks are visible at a broader temperature range for the pulps, which could also be related to the longer chain length.

Upon warming, the power-law and network contribution for pulps are considerably smaller compared to that before cooling but were still present after the freeze-thaw cycle. Moreover the residual structures seems to be swelling in the same temperature range as seen during cooling. For pulp IV400 the remaining contribution from the network structure after a full freeze- thawing cycle is significant and pointing at a poor dissolution (Fig. 6 b blue dashed line). For the remaining cellulose structure it can be connected to the lack of stirring in the system.

The dissolution of pulp IV200 was also performed with different solvent compositions. As shown in Fig. 8, a consistent concentration and ZnO impacts were observed for pulp, as those to MCC (see section, Fig. 4), i.e. higher NaOH concentration and addition of ZnO will promote the dissolution. This is supported by the disruption of the crystalline structure observed by WAXS (see Fig. 8 h), and the hierarchical structure evolution by SAXS. For the pulp fibers, a temperature below 0°C is needed to induce rapid dissolution in the 6.5% NaOH solutions, which is significantly lower than $5-10$°C observed for MCC.

The difference in pulp dissolution behaviour in different solvents is the most pronounced in the thawing, as for the pulp the mesoscale component retain the apparent contribution after dissolving. Thus, it can be assumed that despite observed swelling, the cellulose structure in the pulp fibers is more resistant to dissolution compared to cellulose in MCC. For the pulp fibers, the dissolution continued during the warming up phase. Before reaching room temperature the network structure disappeared. As for MCC, the addition of ZnO improved the dissolution by favoring a faster dissolution rate and possibly fewer residual crystalline structures.

In the dilute solvents, the 4% NaOH concentrations, the dissociation does not occur before ice formation, similar to what was observed for MCC. In addition, despite a significantly reduced contribution from the larger scale and network above 0°C, a small portion of the network structures remained due to the lack of stirring as aforementioned. The fitted radius of gyration value is consistently around 1 nm.

## Dissolution of agricultural-based pulps

The bleached oat and wheat pulps do not fully dissolve and their dissolution profiles is very different compared to the wood based pulps. Despite their low intrinsic viscosity, they remain undissolved. Bleached oat and wheat pulps consist of both cellulose I and cellulose II, probably due to high NaOH content present during oxygen bleaching(see Fig. 2). The Bragg reflections of (102) and (200) of cellulose I and those of (110) and (020) of cellulose II are

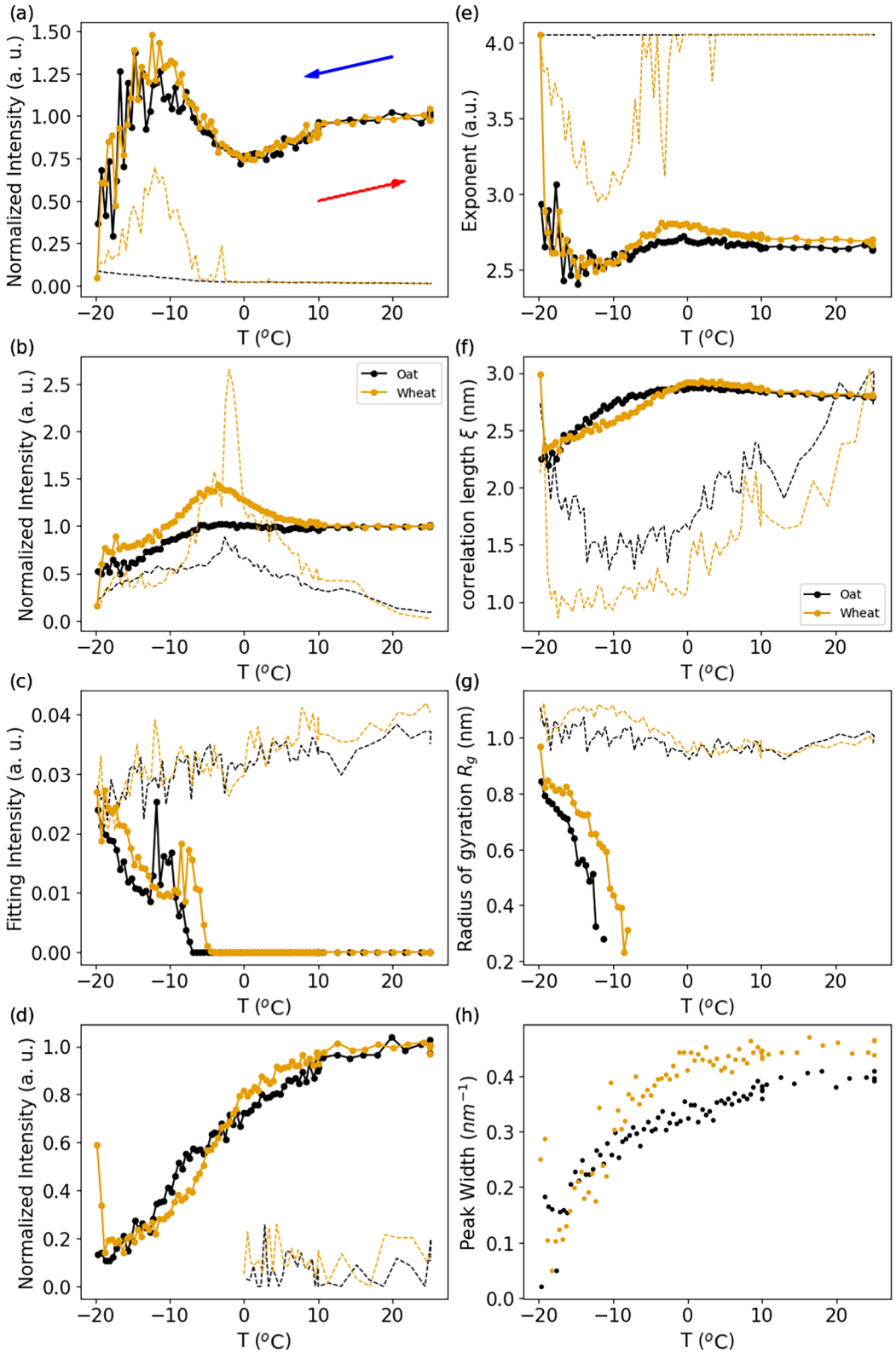
(a)
Normalized Intensity (a. u.)
T (°C)
(b)
Normalized Intensity (a. u.)
Oat
Wheat
T (°C)
(c)
Fitting Intensity (a. u.)
T (°C)
(d)
Normalized Intensity (a. u.)
T (°C)
(e)
Exponent (a.u.)
T (°C)
(f)
correlation length ξ (nm)
Oat
Wheat
T (°C)
(g)
Radius of gyration $R_g$ (nm)
T (°C)
(h)
Peak Width ($nm^{-1}$)
T (°C)

◂**Fig. 9** Summaries of SAXS and WAXS fitting parameters of bleached Oat (black) and Wheat (blue) in 6.5% NaOH and 1.3% ZnO. **a-c** and **e-g** show the same parameters as those in Fig. 4. **d** and **e** are the evolution of the intensities and peak positions of WAXS Cel I (200)/Cel II (020). The solid lines with circles present the cooling cycles marked by the solid blue arrow in **a**, while the dashed lines stand for heating cycles marked by the red arrow in **a**

overlapped, showing two broad features with comparable intensities. Instead of assigning the contribution of each Bragg reflection, two Voigt functions were used to approximate the profile qualitatively. Figure 9 shows the disruption of the crystalline structure for these cereal pulps, with a similar decay to MCC and pulps. To make the discussion simpler, we only plot the development of the peak which mainly consists of cellulose I (200) and cellulose II (020) reflections in Fig. 9 d.

For the cooling part, their WAXS peak intensity decay compared to that of wood-based pulps shows a much smoother (or slower) decay trend, which may stem from their distinct crystalline structures. However, the hierarchical structure did not show simple stepwise decay for power-law contribution with nevertheless the onset still around 10°C. A local maximum of the intensity of the network correlation length is still observed for wheat, like MCC and pulps, but less pronounced. This is not the case for bleached oats where no peaked intensity is observed in all NaOH and ZnO solutions (see supplementary information ). Such a difference may be related to the higher cellulose II composition in bleached wheats and oats, which is more stable than cellulose I in aqueous NaOH solutions (Budtova and Navard 2016; Lindman et al. 2017). What is interesting is the consistent radius of gyration around 1 nm of the smaller objects even for bleached oat and wheat, perhaps due to a slightly simplified Guinier fitting function. Nevertheless, these formed objects accompanied by the disintegration of crystalline structures probably don't retain the crystalline form as before dissolution. The impact of the solution composition to bleached oat and wheat is in line with those to MCC and pulps. Addition of ZnO promotes the dissolution rate but the concentration difference between 6.5% and 4% is not as strong as for MCC and the pulps (See Supplementary information).

## Conclusions

The in-situ WAXS and SAXS results allowed to visualise multiscale structure changes happening during the cooling down of MCC, wood-based pulps and bleached agricultural celluloses suspension in aqueous NaOH solution. The 6.5 %NaOH with and without ZnO allows partial nanostructural dissociation of cellulose fibres with remaining aggregate structures. Very limited dissolution can be achieved with NaOH concentration less than 6.5%. For MCC and wood-based pulps the dissolution starts with gradual swelling around 10°C and is followed by more rapid disarrangement at a lower temperature, showing the disruption of the crystalline structure. The shorter cellulose chains were easier to dissolve while the presence of fibre structure seemed to hinder the disentanglement of the chains. A clear network expansion has been observed for MCC and wood-based pulps but not as pronounced for bleached oat and wheat pulps. This may be related the presence of cellulose II in the latter, which is more stable in NaOH. The presence of ZnO allowed more efficient dissolution and achieving more stable solutions, meanwhile, the addition of ZnO may lead to the formation of fewer but larger crystalline domains of cellulose during the dissolution according to the WAXS peak width. Cellulose chains could thereafter be identified going into the solution in the form of stiff rods. The crystalline disintegration was visible also in a optical microscopy. In addition,the SAXS-analysis allowed to see that some agglomerated structures remained undissolved at the given experimental conditions.

**Acknowledgements** We acknowledge the financial supports by Vinnova and the Industrial Graduate School Resource-smart Processes under Bioinnovation, with additional funding from TreeToTextile AB, Chalmers University of Technology, and support from Stora Enso. BioInnovation is a strategic innovation program founded by Skogsindustrierna, IKEM and TEKO. The programme is funded by Vinnova, the Swedish Energy Agency and Formas within the framework of the joint initiative Strategic Innovation Areas. We acknowledge DESY (Hamburg, Germany), a member of the Helmholtz Association HGF, for the provision of experimental facilities. Parts of this research were carried out at PETRA III and we would like to thank Dr. Xiao Sun for assistance in using P62 SAXSMAT Beamline. Beamtime was allocated for proposal I-20220167 EC. The Swedish NMR Centre is acknowledged for spectrometer time.

Dr. Kerstin Jedvert is acknowledged for the help with sample preparations.

**Funding** Open access funding provided by RISE Research Institutes of Sweden. This project was financed by Vinnova (2021-03829) and the Industrial Graduate School Resource-smart Processes under Bioinnovation (2021–0923).

**Declarations**

**Conflict of interest** The authors declare no competing interests.

**Ethical Approval** The declaration of ethical approval is not applicable.



## References

Alves L, Medronho B, Antunes FE, Topgaard D, Lindman B (2016) Dissolution state of cellulose in aqueous systems. 1. alkaline solvents. Cellulose 23:247–258

Ashiotis G, Deschildre A, Nawaz Z, Wright JP, Karkoulis D, Picca FE, Kieffer J (2015) The fast azimuthal integration Python library: pyFAI. J Appl Crystallogr 48:510–519

Bialik E, Stenqvist B, Fang Y, Östlund A, Furó I, Lindman B, Lund M, Bernin D (2016) Ionization of cellobiose in aqueous alkali and the mechanism of cellulose dissolution. J Phy Chemistry Letters 7(24):5044–5048. https://doi.org/10.1021/acs.jpclett.6b02346

Budtova T, Navard P (2016) Cellulose in NaOH–water based solvents: a review. Cellulose 23:5–55. https://doi.org/10.1007/s10570-015-0779-8

Cai J, Zhang L (2005) Rapid dissolution of cellulose in LiOH/urea and NaOH/urea aqueous solutions. Macromol Biosci 5:539–548

Cheng G, Zhang X, Simmons B, Singh S (2015) Theory, practice and prospects of x-ray and neutron scattering for lignocellulosic biomass characterization: towards understanding biomass pretreatment. Energy Environ Sci 8:436–455. https://doi.org/10.1039/C4EE03147D

Ciccariello S, Goodisman J, Brumberger H (1988) On the Porod law. J Appl Crystallography 21(2):117–128. https://doi.org/10.1107/S0021889887010409

Cuissinat C, Navard P (2006) Swelling and dissolution of cellulose part ii: Free floating cotton and wood fibres in naoh-water-additives systems. Macromolecular Symposia 244(1):19–30 https://doi.org/10.1002/masy.200651202,https://onlinelibrary.wiley.com/doi/abs/10.1002/masy.200651202

Davidson GF (1937) The dissolution of chemically modified cotton cellulose in alkaline solutions. part 3. in solutions of sodium and potassium hydroxide containing dissolved zinc, beryllium and aluminium oxides. Journal of the Textile Institute Transactions 28(2):T27–T44, https://doi.org/10.1080/19447023708631789

Essity (2021) Essity begins tissue production from alternative fibers, press release

Gubitosi M, Asaadi S, Sixta H, Olsson U (2021) The colloidal structure of a cellulose fiber. Cellulose 28(5):2779–2789. https://doi.org/10.1007/s10570-021-03711-2

Guccini V, Yu S, Agthe M, Gordeyeva K, Trushkina Y, Fall A, Schütz C, Salazar-Alvarez G (2018) Inducing nematic ordering of cellulose nanofibers using osmotic dehydration. Nanoscale 10:23157–23163. https://doi.org/10.1039/C8NR08194H

Fournet Guinier G A (1955) Small-angle Scattering of X-rays. John Wiley & Sons. https://doi.org/10.1107/S0021889891003400

Gunnarsson M, Hasani M, Bernin D (2019) The potential of magnetisation transfer NMR to monitor the dissolution process of cellulose in cold alkali. Cellulose 26:9403–9412. https://doi.org/10.1007/s10570-019-02728-y

Guo S, Li X, Zhao R, Gong Y (2021) Comparison of life cycle assessment between lyocell fiber and viscose fiber in china. International Journal of Life Cycle Assessment 26:1545–1555 10.1016/j.carbpol.2022.119541, https://www.sciencedirect.com/science/article/pii/S0144861722004465

Haemmerle FM (2011) The cellulose gap (the future of cellulose fibres). Lenzinger Berichte 89(1):12–21

Hagman J, Gentile L, Jessen CM, Behrens M, Bergqvist KE, Olsson U (2017) On the dissolution state of cellulose in cold alkali solutions. Cellulose 24(5):2003–2015. https://doi.org/10.1007/s10570-017-1272-3

Jahan MS, Rahman MM, Sutradhar S, Quaiyyum MA (2018) Fractionation of rice straw for producing dissolving pulp in biorefinery concept. Nordic Pulp I & Paper Res J 30:562

Kihlman M, Medronho BF, Romano AL, GermgÅrd U, Lindman B (2013) Cellulose dissolution in an alkali based solvent: influence of additives and pretreatments. J Braz Chem Soc 24:295–303. https://doi.org/10.5935/0103-5053.20130038

Kim T, Kim D, Park Y (2022) Recent progress in regenerated fibers for "green'' textile products. J Cleaner Production 376:134226

Koistinen A, Phiri J, Kesari KK, Vuorinen T, Maloney T (2023) Effect of pulp prehydrolysis conditions on dissolution and regenerated cellulose pore structure. Cellulose 30(5):2827–2840. https://doi.org/10.1007/s10570-023-05050-w

Lindman B, Medronho B, Alves L, Costa C, Edlund H, Norgren M (2017) The relevance of structural features of cellulose and its interactions to dissolution, regeneration,

gelation and plasticization phenomena. Phys Chem Chem Phys 19:23704–23718. https://doi.org/10.1039/C7CP02409F

Liu W, Budtova T, Navard P (2011) Influence of ZnO on the properties of dilute and semi-dilute cellulose-NaOH-water solutions. Cellulose 18(4):911–920. https://doi.org/10.1007/s10570-011-9552-9

Ma Y, Hummel M, Kontro I, Sixta H (2018) High performance man-made cellulosic fibres from recycled newsprint. Green Chem 20:160–169. https://doi.org/10.1039/C7GC02896B

Mao Y, Liu K, Zhan C, Geng L, Chu B, Hsiao BS (2017) Characterization of nanocellulose using small-angle neutron, x-ray, and dynamic light scattering techniques. The Journal of Physical Chemistry B 121(6):1340–1351. https://doi.org/10.1021/acs.jpcb.6b11425

Martin-Bertelsen B, Andersson E, Köhnke T, Hedlund A, Stigsson L, Olsson U (2020) Revisiting the dissolution of cellulose in NaOH as "Seen" by X-rays. Polymers 12(2):342. https://doi.org/10.3390/polym12020342

Mendes IS, Prates A, Evtuguin DV (2021) Production of rayon fibres from cellulosic pulps: state of the art and current developments. Carbohydr Polym 273:118466

Mildner DFR, Hall PL (1986) Small-angle scattering from porous solids with fractal geometry. J Phy D: Appl Phy 19(8):1535. https://doi.org/10.1088/0022-3727/19/8/021

Määttänen M, Gunnarsson M, Wedin H, Stibing S, Olsson C, Köhnke T, Asikainen S, Vehviläinen M, Harlin A (2021) Pre-treatments of pre-consumer cotton-based textile waste for production of textile fibres in the cold NaOH(aq) and cellulose carbamate processes. Cellulose 28:3869–3886. https://doi.org/10.1007/s10570-021-03753-6

Penttilä PA, Rautkari L, Österberg M, Schweins R (2019) Small-angle scattering model for efficient characterization of wood nanostructure and moisture behaviour. J Appl Crystallography 52(2):369–377. https://doi.org/10.1107/S1600576719002012

Penttilä PA, Várnai A, Fernández M, Kontro I, Liljeström V, Lindner P, Siika-aho M, Viikari L, Serimaa R (2013) Small-angle scattering study of structural changes in the microfibril network of nanocellulose during enzymatic hydrolysis. Cellulose 20(3):1031–1040. https://doi.org/10.1007/s10570-013-9899-1

Porod G (1949) Theorie der diffusen röntgenkleinwinkelstreuung an kolloiden systemen. Zeitschrift für Naturforschung A 4(6):401–414. https://doi.org/10.1515/zna-1949-0601

Qi H, Chang C, Zhang L (2008) Effects of temperature and molecular weight on dissolution of cellulose in NaOH/urea aqueous solution. Cellulose 15(6):779–787. https://doi.org/10.1007/s10570-008-9230-8

Saurel D, Segalini J, Jauregui M, Pendashteh A, Daffos B, Simon P, Casas-Cabanas M (2019) A SAXS outlook on disordered carbonaceous materials for electrochemical energy storage. Energy Storage Materials 21:162–173 https://doi.org/10.1016/j.ensm.2019.05.007,https://www.sciencedirect.com/science/article/pii/S2405829719302399

Schmidt PW (1991) Small-angle scattering studies of disordered, porous and fractal systems. J Appl Crystallography 24(5):414–435. https://doi.org/10.1107/S0021889891003400

Schmidt RF, Prévost S, Gradzielski M, Zemb T (2023) Structure of microemulsions in the continuous phase channel. The European Phy J E 46(9):76. https://doi.org/10.1140/epje/s10189-023-00337-z

Shen L, Worrell E, Patel MK (2010) Environmental impact assessment of man-made cellulose fibres. Resources, Conservation and Recycling 55:260–274

Swensson B, Lages S, Berke B, Larsson A, Hasani M (2021) Scattering studies of the size and structure of cellulose dissolved in aqueous hydroxide base solvents. Carbohydr Polym 274:118634. https://doi.org/10.1016/j.carbpol.2021.118634

Teixeira J (1988) Small-angle scattering by fractal systems. J Appl Crystallography 21(6):781–785. https://doi.org/10.1107/S0021889888000263

Teubner M, Strey R (1987) Origin of the scattering peak in microemulsions. The Journal of Chemical Physics 87(5):3195–3200. https://doi.org/10.1063/1.453006

The Fiber Year G (2022) World survey on textiles and nonwovens

Tu H, Li X, Liu Y, Luo L, Duan B, Zhang R (2022) Recent progress in regenerated cellulose-based fibers from alkali/urea system via spinning process. Carbohydr Polym 296:119942. https://doi.org/10.1016/j.carbpol.2022.119942

Väisänen S, Ajdary R, Altgen M, Nieminen K, Kesari KK, Ruokolainen J, Rojas OJ, Vuorinen T (2021) Cellulose dissolution in aqueous NaOH–ZnO: cellulose reactivity and the role of ZnO. Cellulose 28(3):1267–1281. https://doi.org/10.1007/s10570-020-03621-9

Vallejos ME, Olmos GV, Taleb MC, Felissia FE, Ehman NV, Peresin MS, Area MC, Maximino MG (2022) Dissolving pulp from eucalyptus sawdust for regenerated cellulose products. Cellulose 29:4645–4659. https://doi.org/10.1007/s10570-022-04581-y

Vehviläinen M, Kamppuri T, Grönqvist S, Rissanen M, Maloney T, Honkanen M, Nousiainen P (2015) Dissolution of enzyme-treated cellulose using freezing–thawing method and the properties of fibres regenerated from the solution. Cellulose 22:1653–1674. https://doi.org/10.1007/s10570-015-0632-0

Wojtasz J, Sjöstedt N, Storm B, Ulefors A, Mammen Parayil M, Nilsson L, Hernández Leal M, Michud A, Östlund Å, Rydberg T, Bernin D (2024) Production of dissolving pulp from agricultural waste, in manuscript

Xi Y, Le ao JB, Ye Q, Lankone RS, Sung LP, Liu Y, (2021) Controlling bicontinuous structures through a solvent segregation-driven gel. Langmuir 37(6):2170–2178. https://doi.org/10.1021/acs.langmuir.0c03472, pMID: 33533619

Zuckerstätter G, Schild G, Wollboldt P, Röder T, Weber HK, Sixta H et al (2009) The elucidation of cellulose supramolecular structure by $^{13}$C CP-Mas NMR. Lenzinger Berichte 87:38–46